A humanized ossicle model of myelofibrosis reveals THPO-driven fibrosis, osteosclerosis and SPP1-dependent microenvironmental remodeling

Hongzhe Li[1], Alba Lillo Sierras[1], Rong Fan[1], Michaela Oeller[2], Katharina Schallmoser[2], Anne Hultquist[3], Stefan Scheding[1,3,4]

[1] Division of Molecular Hematology and Stem Cell Center, Lund University, Lund, Sweden

[2] Department of Transfusion Medicine, Paracelsus Medical University, Salzburg, Austria

[3] Department of Pathology, Skane University Hospital, Lund University, Lund, Sweden

[4] Department of Hematology, Skane University Hospital, Lund, Sweden

[4] Corresponding author, mail: stefan.scheding@med.lu.se, phone: +46 46 222 33 31

Abstract

Myelofibrosis (MF) is the most severe myeloproliferative neoplasm, and current therapies rarely reverse bone marrow fibrosis, highlighting the need for improved disease models and therapeutic targets. Here, we established a humanized MF model by transplanting thrombopoietin (THPO)-overexpressing human bone marrow $CD34^+$ cells into humanized bone marrow ossicles generated in immunodeficient NSG mice. THPO overexpression induced progressive reticulin fibrosis in vivo, accompanied by myeloid skewing, increased megakaryocyte clustering, and redistribution of human hematopoietic cells to murine spleen and femur, consistent with extramedullary hematopoiesis. THPO-driven ossicles also exhibited features of osteosclerosis, including increased trabecular bone and osteoid formation, indicating active pathological remodeling of the niche. Mechanistically, fibrosis was associated with increased SPP1/OPN expression, which was also observed in bone marrow biopsies from MF patients. Importantly, in vivo neutralization of SPP1 attenuated myeloid skewing, reduced megakaryocyte expansion, and decreased fibrosis severity, highlighting SPP1-driven niche remodeling as a potential therapeutic target in MF.

This humanized MF model thus provides a translationally relevant platform to dissect microenvironment-driven MF pathogenesis and evaluate targeted therapies.

Keywords

Myelofibrosis (MF), humanized MF model, thrombopoietin (THPO), SPP1/OPN

Introduction

Myelofibrosis (MF) is a chronic myeloproliferative neoplasm (MPN) characterized by clonal expansion of hematopoietic stem and progenitor cells (HSPCs), bone marrow (BM) fibrosis, extramedullary hematopoiesis, progressive cytopenias and osteosclerosis [1, 2]. MF is the most aggressive form among the BCR-ABL1-negative MPNs with a considerable risk for transformation to acute leukemia. MF can occur de novo as primary myelofibrosis (PMF) or evolve from essential thrombocythemia (ET) or polycythemia vera (PV) as post-ET and post-PV myelofibrosis, respectively. Driver mutations in Janus kinase 2 (JAK2), calreticulin (CALR), or myeloproliferative leukemia virus oncogene (MPL) are central to MF pathogenesis, leading to constitutive JAK-STAT signaling and dysregulated cytokine production, which drive abnormal megakaryopoiesis, stromal remodeling, and reticulin fiber formation [3].

Despite the introduction of JAK inhibitors such as ruxolitinib, current therapies for MF are largely supportive [4]. JAK inhibitors provide mainly symptomatic relief and reduce splenomegaly but have limited impact on bone marrow fibrosis and disease progression. Although a number of novel MF therapies are under development, allogeneic stem cell transplantation (allo-HSCT) is currently the only curative treatment. Allo-HSCT, however, is a viable option for only a minority of patients due to the higher age of the MF population and corresponding high transplant-related morbidity and mortality. Thus, there is an urgent need for the development of improved therapeutic strategies based on targeting key pathophysiological mechanism in MF.

Here, murine MF models, which are based on thrombopoietin (THPO) overexpression and MPN driver mutation expression, respectively, provide valuable insights into MF pathophysiology and have been widely used for MF drug development [5-10]. However,

species-specific differences in cytokine signaling, megakaryocyte biology, and stromal responses limit their translational relevance.

We therefore aimed to establish a humanized xenotransplantation model that more closely reflects human MF pathology. We generated humanized BM tissues (ossicles) in immunodeficient NSG mice by subcutaneous transplantation of human BM stromal cells followed by intra-ossicle (i.o.) transplantation of THPO overexpressing human CD34 BM cells to induce fibrosis (MF-ossicles). Here, our results demonstrate that the model reproduced key MF features and that novel anti-fibrosis targets could be identified and functionally validated in-vivo.

Thus, this novel MF-ossicle model provides a unique and physiologically relevant platform to study MF pathogenesis and to evaluate therapeutic responses, potentially offering valuable insights for the development of more effective treatments for MF.

Materials and Methods

Human bone marrow mononuclear cell isolation and stromal cell culture

Human bone marrow (BM) samples were obtained from consenting healthy adult donors at the Hematology Department, Skåne University Hospital, Lund, Sweden, through aspiration from the iliac crest, as previously described [11]. In brief, 60 mL of BM were aspirated from each donor into heparin-containing syringes. The procedure was approved by the Regional Ethics Review Board in Lund, Sweden.

Bone marrow mononuclear cells (BM-MNCs) were isolated by density gradient centrifugation using LSM 1077 Lymphocyte separation medium (PAA, Pasching, Austria). BM-MNCs were cultured as previously described [12]. Briefly, cells were resuspended in pre-warmed α-modified minimum essential medium (α-MEM; Sigma-Aldrich, St. Louis,

MO), supplemented with 10% pooled human platelet lysate (pHPL, produced by the Department of Transfusion Medicine, Paracelsus Medical University, Salzburg, Austria), and seeded into tissue culture vessels. After initial incubation, non-adherent cells were removed by washing with phosphate-buffered saline (PBS), and adherent BM stromal cells (MSCs) were subsequently expanded until the required cell number was reached.

Humanized ossicle formation and human hematopoietic cell transplantation

Passage 2-3 cultured human BM-MSCs were harvested by trypsinization (Gibco, Thermo Fisher Scientific). A total of 2×10^6 stromal cells were resuspended in 60 µL of pooled human platelet lysate (pHPL) and mixed with 240 µL of Matrigel-equivalent matrix (In Vitro Angiogenesis Assay Kit, Merck) plus Endothelial Cell Growth supplement (ECGS, Discovery labware Inc) to obtain a final volume of 300 µL per injection. The cell–matrix mixture was then injected subcutaneously into both flanks of 7–8-week-old immunodeficient NOD.Cg-Prkdc^{scid}Il2rγ^{tm1Wjl}/SzJ (NSG) mice (Jackson Laboratory, Bar Harbor, ME) to generate humanized ossicles (two ossicles per mouse).

Beginning on day 3 after implantation, mice received daily subcutaneous injections of human parathyroid hormone (PTH (1–34); 40 µg/kg body weight) into the dorsal neck fold for 28 days to promote bone formation. Eight weeks after stromal cell implantation, ossicle-bearing mice were subjected to sublethal irradiation (200 cGy). At least four hours after irradiation, $1–3 \times 10^5$ human BM CD34$^+$ cells—either non-transduced, lentiviral GFP-transduced, or lentiviral THPO-GFP-transduced—were injected directly into each ossicle.

Generally, mice were euthanized eight weeks after CD34$^+$ cell transplantation, and tissues including ossicles, spleen, femurs, and liver were collected for downstream analyses. For time course fibrosis analysis, selected groups of mice were analyzed after 4 - 10 weeks. All

animal experiments were performed in accordance with institutional and national ethical guidelines and were approved by the Malmo/Lund ethics committee for animal research.

Lentiviral transduction of BM CD34$^+$ Cells

MACS-enriched human bone marrow CD34$^+$ cells were cultured overnight in StemSpan SFEM (StemCell Technologies, Vancouver, BC, Canada) supplemented with recombinant human SCF, THPO, and FLT3L (each at 100 ng/mL; PeproTech, Rocky Hill, NJ, USA). The following day, CD34$^+$ cells were transduced with lentiviral particles encoding either THPO-GFP or GFP control at a multiplicity of infection (MOI) of 5. The lentiviral expression plasmids (THPO-GFP and GFP control) and the corresponding viral preparations were generated by the Cell and Gene Technologies Core Facility at the Lund Stem Cell Center. Twenty-four hours after transduction, cells were collected, washed, resuspended in PBS, and used for in vivo transplantation.

In vivo antibody administration

Anti-human SPP1/OPN antibody and corresponding isotype control antibody, respectively (both at 15 mg/kg body weight; Bioxcell, Lebanon, NH, USA) were administered via intraperitoneal injection. Treatment was initiated at week 4 and continued once weekly for two weeks. From week 6 onward, anti-human SPP1/OPN antibody was administered twice weekly until the experimental endpoint. Antibody doses and administration schedules were selected based on previously published studies [13, 14].

Cell isolation from ossicles, femur, spleen, and liver

At indicated time points after intraossicle transplantation of human BM CD34$^+$ cells, mice were euthanized and ossicles, spleens, femurs, and livers were collected for cell isolation.

Ossicles: Each ossicle was mechanically dissociated using a mortar and pestle, followed by enzymatic digestion in ossicle digestion buffer (Phosphate Buffered Saline, PBS, containing 5% Fetal Bovine Serum, FBS, 2 mg/mL collagenase II, and 4 mg/mL dispase II; 5 mL per ossicle) at 37 °C for 1 h with gentle agitation. The digested suspension was passed through a 100-µm cell strainer, and enzymatic activity was quenched by adding 35 mL of ice-cold PBS supplemented with 10% FBS. Cells were pelleted by centrifugation, washed twice with PBS + 10% FBS, and centrifuged again.

Spleen and liver: Tissues were mechanically dissociated by cutting them into small fragments, followed by gentle crushing and repeated pipetting in PBS to obtain single-cell suspensions.

Femur: After removal of both femoral heads, bone marrow was flushed from the diaphysis using a syringe and needle with 10 mL PBS + 5% FBS. The remaining femoral shafts and heads were then cut into small fragments and further dissociated using a mortar and pestle.

Cells isolated from ossicles, spleen, liver, and femur were subjected to red blood cell (RBC) lysis prior to antibody staining. RBC lysis was performed using 1× Pharm Lyse (BD Biosciences) according to the manufacturer's instructions.

Flow cytometry

Cells isolated from the different tissues were incubated in blocking buffer [Dulbecco's PBS w/o Ca2+, Mg2+, 3.3 mg/ml human normal immunoglobubin (Gammanorm, Octapharm, Stockholm, Sweden), 1% FBS (Invitrogen, city, Country)], followed by staining with antibodies against human CD45, CD15, CD33, CD66b, CD19, CD41a, CD42b, CD34, CD56 and CD271. Antibodies are listed below. Gates were set according to the corresponding fluorescence-minus-one (FMO) controls and cells were analysed on Symphony A1 (BD

Bioscience, Erembodegem, Belgium). Dead cells were excluded by DAPI (Merck) staining and doublets were excluded by gating on FSC-H versus FSC-W and SSC-H versus SSC-W.

Antibodies

For FACS analysis, the following antibodies were used: hCD45-APC (clone HI30, BD Pharmingen), hCD15-PE (clone HI98, BD Pharmingen), hCD33-PE (clone P67.6, BD), hCD66b-PE (clone G10F5, BD Pharmingen), hCD19-PE-Cy5 (clone HIB19, BD Pharmingen), hCD41a-PE (clone HIP8, BD), CD42b-APC (clone HIP1, BD), hCD34-PerCP-Cy5.5 (clone 8G12, BD), hCD271-APC (ME20.4-1.H4, Miltenyi Biotec), hCD45-APC-Cy7 (clone 2D1, BD Pharmingen).

Hematoxylin and Eosin (H&E) Staining

Paraformaldehyde-fixed, paraffin-embedded (FFPE) tissue sections were deparaffinized in Neo-Clear (2 × 5 min) and rehydrated through a graded ethanol series (2 × 5 min in 100% ethanol, 2 × 5 min in 95% ethanol, 1 × 5 min in 70% ethanol), followed by 2 × 5 min rinses in Milli-Q (MQ) water. Sections were stained with hematoxylin for 1 minute, rinsed in tap water for 2 minutes, and briefly dipped in acid alcohol to remove excess stain. After a 10-minute rinse in running tap water, slides were counterstained with eosin for 30 seconds, followed by rinsing in tap water (2 min) and MQ water (2 min). Dehydration was performed through a reverse ethanol gradient (1 × 2 min in 70%, 2 × 3 min in 95%, and 2 × 3 min in 100% ethanol), followed by clearing in Neo-Clear (2 × 5 min). Coverslips were mounted using a xylene-based mounting medium and allowed to dry at room temperature.

Gordon and Sweet's Reticulin Staining

Paraformaldehyde-fixed, paraffin-embedded (FFPE) tissue sections were incubated at 60 °C for 20 minutes, followed by deparaffinization in Neo-Clear (two changes, 5 minutes each). Slides were rehydrated through a graded ethanol series: two changes of absolute ethanol (3

minutes each), two changes of 95% ethanol (2 minutes each), and finally immersed in Milli-Q (MQ) water for 3 minutes.

Slides were then oxidized in acidified potassium permanganate solution (2 mL 3% sulfuric acid + 48 mL 0.5% potassium permanganate) for 1 minute and rinsed twice in MQ water (1 minute each). Bleaching was performed by dipping the slides into 1% oxalic acid for 30 seconds, followed by immersion in tap water for 3 minutes. After two additional washes in MQ water (1 minute each), slides were incubated in 2.5% ferric ammonium sulfate for 20 minutes and rinsed three times in distilled water (2 minutes each).

Meanwhile, the diamond-silver solution was prepared as follows: 25% ammonium hydroxide was added dropwise to 5 mL of 10% silver nitrate solution until the mixture turned clear. Next, 5 mL of 3% sodium hydroxide was added, followed by additional ammonium hydroxide until the solution cleared again. Finally, 40 mL of MQ water was added, and the solution was filtered before use.

Following the ferric ammonium sulfate incubation, slides were immersed in the freshly prepared diamond-silver solution for 25 seconds, rinsed with MQ water for 1 minute, and incubated in 10% formaldehyde for 1 minute. Slides were then washed in tap water for 5 minutes.

Counterstaining was performed using 0.04% gold chloride for 90 seconds. Excess stain was removed by rinsing with tap water for 2 minutes followed by immersion in 5% sodium thiosulfate for 5 minutes. Slides were then washed in tap water (three times, 2 minutes each), stained with nuclear fast red for 7 minutes, and dehydrated through a graded ethanol series: MQ water (2 changes, 2 minutes each), 95% ethanol (2 changes, 2 minutes each), and absolute ethanol (2 changes, 2 minutes each), followed by clearing in Neo-Clear (2 changes, 3 minutes each). Coverslips were mounted using a xylene-based mounting medium, and

slides were allowed to dry at room temperature for at least one hour. Fibrosis grading was independently performed in a blinded manner to minimize evaluation bias.

Trichrome RGB Staining

The RGB trichrome staining was performed based on the protocol by Gaytan et al. (2020) [15] with minor modifications. Paraformaldehyde-fixed, paraffin-embedded (FFPE) tissue sections were first incubated in a dry oven at 60 °C for 45 minutes to facilitate deparaffinization. Slides were then deparaffinized in Neo-Clear (two washes, 5 minutes each) and rehydrated through a graded ethanol series: two washes in absolute ethanol (5 minutes each), two washes in 95% ethanol (5 minutes each), one wash in 70% ethanol (5 minutes), followed by two washes in Milli-Q water (5 minutes each).

Slides were stained with 1% Alcian Blue 8GX in 3% aqueous acetic acid (pH 2.5) for 30 minutes and rinsed in tap water for 5 minutes. This was followed by staining with 0.04% Fast Green FCF in Milli-Q water for 20 minutes. After another 5-minute rinse in tap water, slides were incubated in 0.1% Sirius Red in 1% acetic acid for 1 hour. Excess stain was removed by rinsing twice in acidified water (1% acetic acid in tap water).

Dehydration was performed through an ascending ethanol series (70% ethanol for 2 minutes, followed by two washes in 95% ethanol and two washes in absolute ethanol, each for 3 minutes). Slides were then cleared in Neo-Clear (two washes, 5 minutes each) and mounted using a xylene-based mounting medium. Slides were allowed to dry at room temperature before imaging.

The immature bone stained red by Sirius Red due to the high content of collagen, while the high deposition of hydroxyapatite in the mineralized bone matrix masked the collagen staining and the mineralized matrix showed a green pigmentation.

Immunohistochemistry (IHC)

Immunohistochemical staining was performed using the SignalStain® IHC Dual Staining Kit (BioNordika, Cat# 82456S) following the manufacturer's instructions with minor modifications.

Tissue preparation: FFPE tissue sections were incubated at 60 °C for 30 min in a dry oven, deparaffinized in Neo-Clear (two washes, 5 min each), and rehydrated through a graded ethanol series: 2 × absolute ethanol (5 min each), 2 × 95% ethanol (5 min each), 1 × 70% ethanol (5 min), followed by 2 × distilled water (5 min each).

Antigen retrieval and blocking: Antigen retrieval was performed by submersing slides in RNAscope® Target Retrieval Buffer (Advanced Cell Diagnostics, Cat# 322000) at 98 °C for 20 min in a steamer. Slides were then rinsed 3 × 5 min with distilled water, circled with a wax pen (ImmEdge® Pen, Vector Laboratories, Cat# H-4000), and treated with BLOXALL® Blocking Solution (Vector Laboratories, SP-6000) for 10 min to quench endogenous peroxidase and alkaline phosphatase activity.

For primary antibody incubation, slides were rinsed with 1× TBST (500 ml Tris-buffered saline [Fisher Scientific, Cat# BP247111] + 500 µl Tween-20 [Sigma-Aldrich, Cat# P1379]) for 5 min. Sections were blocked with 10% goat serum in TBST (Jackson ImmunoResearch, Cat# 005-000-121) for 1 h at room temperature. After washing 2 × with dH_2O and 1 × with TBST (5 min each), slides were incubated with Mouse-on-Mouse IgG Blocking Solution (Invitrogen, Cat# R37621) for 1 h. Sections were then incubated overnight at 4 °C with a primary antibody cocktail in PBS + 5% goat serum containing anti-CD61 (mouse monoclonal, clone ZM33, Zeta Corporation, 1:400) and anti-human mitochondria (rabbit monoclonal, clone MTC02/2860R, Fisher Scientific, 1:50)

For secondary detection and color development, sides were washed 3 × 5 min with TBST, incubated with HRP Boost Detection Reagent for 30 min at room temperature, and visualized

using DAB substrate (SignalStain® DAB Chromogen: 30 µl + 1 ml diluent). After 3 × 5 min washes, slides were treated with AP Boost Detection Reagent for 30 min at room temperature, followed by Alkaline Phosphatase (AP) Vibrant Red substrate development (SignalStain® Vibrant Red Reagent 1 & 2: 1 drop each + 2.5 ml diluent) for 20 min. Slides were then rinsed 2 × 5 min with distilled water and counterstained with Mayer's hematoxylin for 1 min, followed by acid-alcohol differentiation and rinsing.

Last, sections were dehydrated through a reverse ethanol series (70%, 95%, 100%), cleared in Neo-Clear (2 × 5 min), and mounted with xylene-based mounting medium.

Bone and megakaryocyte quantification

H&E-stained slides were scanned using an Olympus VS120 scanner. Digital images (.vsi) were exported as .tif using OlyVIA 3.3 (Olympus, Build 24382) and imported into QuPath v0.5.1 for analysis.

For bone quantification, whole tissue sections were analysed using a single-intensity threshold of 0.02 for the eosin channel, with manual corrections using wand and brush tools as needed. A training image for the bone pixel classifier was annotated for bone, cells, and background, then trained using an artificial neural network (ANN_MLP). Classification accuracy was visually assessed; areas not optimally recognized were measured manually. Bone area was normalized to total ossicle area.

The number of megakaryocytes was normalized to cavity area (total area minus bone area). Megakaryocyte clusters were defined as 3–5 adjacent megakaryocytes without interstitial cells [16] and manually counted in QuPath.

Immunofluorescence staining

FFPE sections were deparaffinized and rehydrated as described above. Antigen retrieval was performed using RNAscope® Target Retrieval Buffer at 98 °C for 15 min. Slides were washed 3 × 5 min with PBS + 0.1% Tween-20, circled with a wax pen, and blocked in PBS containing 10% goat and donkey serum for 1 h at room temperature. Sections were incubated overnight at 4 °C with primary antibodies in PBS with goat anti-human OPN (SPP1, 1:150) and rabbit anti-human CD56 (1:200). Slides were washed 3 × 5 min with PBS and incubated with secondary antibodies for 1 h at room temperature (donkey anti-goat AF647, 1:200; goat anti-rabbit AF488, 1:200). After 3 PBS washes, nuclei were counterstained with DAPI (1 μg/ml) for 10 min. Sections were mounted with ProLong™ Gold Antifade Mountant and imaged using a Leica STELLARIS confocal microscope with the following settings: AF647 (SPP1) 647 nm, AF488 (CD56) 488 nm, DAPI 405 nm.

Results

Establishment of a humanized bone marrow microenvironment in NSG mice

To establish an ectopic humanized bone marrow (BM) niche capable of supporting human hematopoiesis, we adopted the approach described by Reinisch et al. [17] (Fig. 1A). Briefly, bone marrow-derived stromal cells from healthy donors were culture-expanded and injected subcutaneously into immunodeficient NSG mice together with an angiogenic hydrogel. Over time, this led to the formation of a bony ossicle (huOssicle) containing functional bone marrow tissue with key anatomical features of human bone marrow including cortical bone, trabecular bone, adipocytes, fibroblastic stroma, and blood vessels (Fig. 1B). We also identified distinct periosteal and endosteal regions and that ossicle BM was infiltrated by murine hematopoietic cell (Fig. 1B). Importantly, staining for human-specific mitochondria confirmed the human origin of osteocytes and stromal elements (Fig. 1C).

In the next step, human $CD34^+$ hematopoietic bone marrow (BM) cells were injected intra-ossically (i.o) into 8-week ossicles. Human $CD45^+$ cell engraftment within the ossicle was detectable as early as 4 weeks post-injection (Fig. S1A). By 8 weeks, human $CD45^-$ cells were observed in the endosteal, peri-adipocytic, and interstitial regions, indicating presence of non-hematopoietic stromal cells within the ossicles (Fig. S1B). Engraftment of human hematopoietic cells was significantly higher in the ossicles compared to the murine femur (48.9% vs. 2.32%, ossicle: n=8, femur: n = 5, p = 0.0016), demonstrating the superior capacity of the humanized ossicle to support human hematopoiesis (Fig. 1D-E). Both human myeloid cells ($CD15^+$, $CD33^+$, $CD66b^+$) and $CD19^+$ lymphoid cells were detected, along with human $CD34^+$ hematopoietic stem and progenitor cells (Fig. S1C, S1D) showing that the humanized BM microenvironment in NSG mice supported robust engraftment and differentiation of human hematopoietic cells.

Ossicles injected with THPO-overexpression CD34+ cells show a skewed myeloid/lymphoid ratio, increased megakaryocytopoiesis and pronounced megakaryocyte clustering

In vitro, THPO overexpression led to an increased percentage of $CD41a^+CD42b^+$ megakaryocytes, even in the absence of exogenous THPO in the culture medium (Fig. S2A and S2B). This result confirmed the functionality of lentiviral THPO overexpression.

Flow cytometry analysis of ossicles showed that both, intraossicle (i.o) injection of GFP- and THPO- overexpressing $CD34^+$ cells resulted in a robust engraftment in the humanized ossicle, with comparable levels of human $CD45^+$ cells (Fig. 2A, S2C). Eight weeks following injection, the fraction of THPO-overexpressing cells was increased compared with the initial frequency at the time of injection compared to controls (Fig. S2D), indicating a more rapid expansion of THPO-overexpressing cells. Moreover, ossicles injected with THPO-

overexpressing $CD34^+$ cells exhibited myeloid skewing, as indicated by a higher ratio of myeloid ($CD15^+$, $CD33^+$, $CD66b^+$) to $CD19^+$ lymphoid cells (Fig. 2B).

Additionally, 8-week huMF ossicles showed a tendency to increased frequencies of $CD41a^+CD42b^+$ megakaryocytes compared to controls (Fig. 2C). However, differences were not statistically significant. In order to corroborate the flow cytometry findings, we quantified the number of human megakaryocytes in H&E-stained FFPE slides. IHC staining with human mitochondria marker showed an increased number of human megakaryocytes in huMF ossicles (Fig. 2D). As shown in Fig. 2E, there was a 1.5-fold increase in total megakaryocytes in huMF ossicles compared with GFP controls. We also found a significantly increased megakaryocytic clustering in huMF ossicles (Fig. 2F).

Transplantation of THPO overexpressing CD34+ bone marrow cells induces myelofibrosis in humanized ossicles

Thrombopoietin (THPO) overexpression has been shown to induce myelofibrosis in murine models [9, 18]. Humanized ossicles were therefore injected with human THPO-GFP bone marrow (BM) $CD34^+$ cells and examined at 4, 5, 6, and 8 weeks after transplantation (i.o.). Staining for reticulin fibers was used as the gold standard to evaluate myelofibrosis using clinically-established criteria [19]. No fibrosis was observed at 4 weeks after transplantation (Fig. S3A), whereas moderate to high-grade (grade 2-3) reticulin fiber deposition became evident at weeks 5 (Fig. S3B) and 6 (Fig. S3C). By 8 weeks, a dense net of reticulin fibers was formed in the THPO ossicle marrow cavity, extending between hematopoietic areas and along trabecular bone surfaces, consistent with stable and well-established fibrosis (Fig. 3A). The median grade of week 8 ossicles engrafted with THPO-overexpressing $CD34^+$ cells was grade 2 and was significantly higher compared to GFP controls (Fig. 3B). Based on these

findings, the 8-week time point was selected for subsequent studies and ossicles were assigned as 8 week huMF ossicles.

THPO overexpression triggers HSPC migration from ossicles to other hematopoietic organs in NSG mice

In 8-week huMF ossicle-bearing mice, we observed an increased percentage of human $CD45^+$ hematopoietic cells in the femur and spleen compared to controls (Fig. 4A-B). Migrated human cells were primarily detected in the femurs, followed by the spleen and, to a much lesser extent, the liver (Fig. 4A-B, S4A-B). This distribution pattern likely reflects the superior hematopoietic-supportive microenvironment of the femur relative to the spleen and liver.

A trend toward increased migration of human hematopoietic cells to the femur was observed in the THPO group (Fig. 4A), which did not reach statistical significance. In contrast, a significantly higher fold change of human hematopoietic cells was detected in the spleens of the THPO group (Fig. 4A), despite comparable spleen sizes and spleen-to-body weight ratios of the THPO and GFP controls (Fig. 4C and S4C).

Together, these findings indicate an enhanced migration of human hematopoietic cells from humanized ossicles to suboptimal hematopoietic niches in the THPO group, suggesting that overexpression of THPO in $CD34^+$ cells caused alterations of the ossicle hematopoietic microenvironment (HME) that favoured migration.

HuMF ossicles exhibit increased osteosclerosis

Another well-recognized feature of myelofibrosis is osteosclerosis. To investigate whether ossicles transplanted with THPO overexpressing $CD34^+$ cells (HuMF ossicles) showed increased bone formation, high-resolution images from scanned H&E-stained slides were

used to quantify the ossicle bone areas. Here, our data demonstrated that huMF ossicles had a higher bone-to-total ossicle area ratio compared to the GFP group, indicating increased bone formation caused by THPO-overexpressing $CD34^+$ cells (Fig. 5A-B). Manual quantification of the trabecular bone area furthermore demonstrated a significant increase in trabecular bone formation in huMF ossicles compared with controls (Fig. 5C).

We further performed trichrome staining (also known as RGB staining) which allowed us to distinguish between different stages of osteogenesis based on the differences in collagen staining patterns between unmineralized bone and mineralized bone matrix. RGB staining demonstrated that cortical bones (outer layer) of the ossicles were mainly composed of the mineralized hardened matrix while the trabecular bones (the porous, lattice-like inner bone) were mostly composed of an unmineralized matrix. i.e. osteoid (Fig. 5D). Here, quantitative analysis demonstrated that huMF ossicles contained a higher percentage of unmineralized osteoid (purple) compared to GFP controls, suggesting a more pronounced microenvironmental remodelling (Fig. 5E).

Collectively, our results show that THPO-driven hematopoietic cells stimulate pathological bone remodeling within the ossicle, reflecting the osteosclerotic changes characteristic of myelofibrosis.

SPP1/OPN Is Upregulated in Myelofibrosis and Its Neutralization Partially Rescues MF Pathology

The enhanced bone formation observed in THPO ossicles suggested an increased activity of human osteoprogenitors within the humanized bone marrow microenvironment. Using single-cell RNA sequencing (scRNA-seq), we have in a previous study identified $CD56^+$ cells as osteochondroprogenitors characterized by exclusive expression of SPP1, which mediates their interactions with hematopoietic cells through an SPP1-dependent signaling axis [20].

Based on these findings, we performed immunostaining for CD56 and SPP1 to assess osteoprogenitor activation in THPO ossicles. Immunofluorescence staining indicated a higher level of SPP1 expression in THPO ossicles compared with GFP controls (Fig. 6A), suggesting enhanced osteoprogenitor activity and matrix production. These findings were confirmed in clinical bone marrow biopsies from patients with primary MF compared with hematologically healthy controls (Fig. 6B). Consistent with our huMF ossicle findings, patient MF samples exhibited significantly higher expression of SPP1/OPN (median SPP1 intensity: 3.38, n = 3) compared with controls (median SPP1 intensity: 2.71, n = 3) (Fig. 6B).

In summary, these findings demonstrate that THPO overexpression in $CD34^+$ cells is associated with enhanced osteogenic ossicle remodeling, accompanied by activation of $CD56^+$ osteoprogenitors, a feature that mirrors pathological bone remodeling observed in myelofibrosis. Importantly, SPP1/OPN was also upregulated in PMF patient biopsies.

To test the functional relevance of SPP1/OPN overexpression, we then went on to treat huMF ossicle mice with anti-SPP1 antibody. The results showed that antibody treatment attenuated the increased myeloid-to-lymphoid ratio (Fig. 6C) and that $CD41^+$ megakaryocyte frequency in huMF ossicles was reduced following anti-SPP1 treatment (Fig. 6D). Importantly, histological analysis revealed a marked reduction of fibrosis in anti-SPP1–treated mice (Fig. 6E). Furthermore, percentages of human $CD45^+$ cells in the spleen showed a trend toward lower levels in anti-SPP1 treated mice (Fig. 6F) and there was also a trend toward reduced bone area following anti-SPP1 administration (Fig. 6G).

Discussion

A number of experimental models have been developed to study myelofibrosis pathogenesis. Murine models based on genetic modification of hematopoiesis including transgenic or retroviral overexpression of THPO [18], $JAK2^{V617F}$ [22], MPL^{W515L} [7], and CALR mutations

[23] recapitulate key disease features. However, because fibrosis develops within an entirely murine microenvironment, these models do not fully capture species-specific stromal responses and niche–hematopoietic cell interactions relevant to the human disease.

To address species differences in hematopoiesis, xenotransplantation models using human mutated HSPCs have been widely adopted. In these models, human $CD34^+$ cells carrying driver mutations are transplanted into immunodeficient mice to study human clonal hematopoiesis in vivo [17, 24]. Although these systems capture cell-intrinsic effects of disease mutations, fibrosis development is often limited, likely due to lacking interactions between human hematopoietic cells and murine stromal cells and potential differences in fibrogenic pathways.

As an alternative, recent advances in stem cell biology have enabled the development of in vitro fibrosis models based on induced pluripotent stem cell (iPSC)-derived organoids [25]. These systems allow a controlled reconstruction of hematopoietic and stromal components, and they are particularly valuable for mechanistic studies and high-throughput drug screening. However, the in vitro nature of this approach limits their ability to fully capture the spatial organization, vascularization, mechanical forces, and, importantly, the long-term remodeling characteristic of bone marrow fibrosis development.

In this context, humanized bone marrow niche models, including ectopic ossicle systems, offer a unique intermediate approach for modeling myelofibrosis in vivo. Humanized bone marrow tissues established in immunodeficient mice enable sustained engraftment of human hematopoietic cells and, thus, allow to study pathological BM remodeling within a species-matched niche.

Accordingly, we herein demonstrate an ossicle-based system that recapitulated key features of myelofibrosis and allowed for a direct investigation of human hematopoietic-stromal crosstalk and therapeutic targeting of niche-derived factors.

We established a humanized bone marrow microenvironment (hu ossicles) in immunodeficient NSG mice by transplantation of human BM stromal cells and showed that overexpression of THPO in human $CD34^+$ cells was sufficient to induce fibrotic ossicles (huMF ossicles). These huMF ossicles showed key hallmarks of myelofibrosis, including myeloid skewing, megakaryocytic dysplasia, progressive reticulin fibrosis, extramedullary hematopoiesis, and pathological bone remodeling.

Importantly, we identify SPP1/OPN as a critical mediator of the pathological changes and showed that SPP1/OPN neutralization partially rescued the myelofibrotic phenotype. Clearly, this finding indicates that the anti-SPP1 antibody approach might present a possible novel therapy for myelofibrosis, which needs to be addressed in future studies.

In the murine system, THPO overexpression leads to rapid and consistent induction of bone marrow fibrosis. We therefore chose to employ THPO overexpression in human CD34+ hematopoietic cells as a first step to induce fibroses in humanized ossicles. Certainly, alternative approaches including generation of huMF ossicles using mutated hematopoietic cells might be possible and will be evaluated in future experiments.

Consistent with murine models of myelofibrosis [18, 26, 27], we saw a trend toward expansion and clustering of megakaryocytes in the THPO ossicles, which is a defining feature of myelofibrosis pathogenesis. Progressive ossicle reticulin fibrosis developed over time and was well-established eight weeks post-transplantation of THPO-overexpressing $CD34^+$ cells. Notably, the spatial distribution and architecture of reticulin fibers in the MF ossicles closely resembled those observed in human myelofibrosis, with dense networks extending between hematopoietic areas and along trabecular bone surfaces. These findings demonstrate that dysregulated THPO signaling in human hematopoietic cells is sufficient to drive fibrotic remodeling within a human stromal context, supporting the notion that hematopoietic cell–intrinsic alterations can initiate and sustain fibrotic niche remodeling.

In myelofibrosis patients, the bone marrow's ability to support hematopoiesis is compromised, leading to a shift of blood cell production to other hematopoietic organs. Consequently, a hallmark feature of myelofibrosis is extramedullary hematopoiesis, often manifested as splenomegaly and hepatomegaly. In parallel with fibrotic progression, we observed enhanced migration of human hematopoietic cells from the humanized ossicles to murine hematopoietic organs, most prominently the spleen. This redistribution mirrors extramedullary hematopoiesis. The relatively low proportion of human hematopoietic cells detected in the spleen may account for the absence of overt splenomegaly at this stage and splenomegaly might develop at later stages as hematopoietic cell accumulation progressively increases, which we however have not investigated yet.

Quantitative analysis revealed increased human $CD45^+$ cell engraftment in both the murine femur and spleen of THPO ossicle–bearing mice compared with controls. This difference likely reflects intrinsic variations in the hematopoietic-supportive capacity of these organs. While the murine femur represents a relatively permissive niche for human hematopoietic cells even under baseline conditions, the spleen acts as a more responsive extramedullary site where pathological cues may drive a more pronounced accumulation of human cells.

Importantly, the preferential accumulation of human hematopoietic cells in the spleen is consistent with a key clinical hallmark of myelofibrosis, which is the mobilization of HSPCs from the BM and their expansion in extramedullary organs. The absence of statistical significance in femoral engraftment does not exclude biologically meaningful migration but rather suggests that niche occupancy or saturation may limit further accumulation.

Osteosclerosis represents another hallmark of myelofibrosis and remains incompletely understood mechanistically. Our data demonstrate that THPO overexpression induced excessive bone formation within the ossicles, characterized by increased trabecular bone area and accumulation of unmineralized osteoid. These findings suggest an imbalance between

bone formation and maturation, indicative of active but dysregulated osteogenesis. The presence of abundant osteoid further implies ongoing microenvironmental remodeling rather than static bone deposition.

Mechanistically, we identified a marked upregulation of CD56 and SPP1/OPN in THPO ossicles, implicating activation of osteochondroprogenitor populations [20]. In line with our previous single-cell transcriptomic analyses, $CD56^+$ cells expressing high levels of SPP1 appear to represent a specialized osteoprogenitor subset that engages in bidirectional crosstalk with hematopoietic cells [20]. The concordant upregulation of CD56 and SPP1 in bone marrow biopsies from primary myelofibrosis patients underscores the clinical relevance of these findings and supports the translational validity of our model. These observations are consistent with recent studies demonstrating that fibrosis-inducing hematopoietic cells can reprogram bone marrow stromal progenitors toward a profibrotic and osteogenic state. In particular, peritrabecular osteolineage cells marked by NCAM1/CD56 have been shown to expand during myelofibrosis and contribute to osteosclerosis through activation of Wnt/β-catenin–dependent programs [28]. The expansion of $CD56^+$ stromal populations observed in our THPO-driven model therefore likely reflects a similar injury-induced stromal remodeling process, in which osteolineage progenitors are activated and progressively occupy the central marrow space. Moreover, SPP1/OPN has emerged as a central profibrotic mediator in myelofibrosis, promoting stromal cell activation and collagen production, correlating with fibrosis severity, and representing a promising therapeutic target [14, 29].

Importantly, therapeutic neutralization of SPP1/OPN attenuated several THPO-induced pathological features, including myeloid skewing, megakaryocyte expansion, and fibrosis severity. Although reductions in splenic engraftment and bone area did not reach statistical significance, the observed trends suggest that longer treatment duration or combination approaches may further enhance therapeutic efficacy, which can be studied in future

experiments. Our findings thus strongly suggest SPP1/OPN not merely as a biomarker of disease-associated stromal activation, but as a functional mediator of hematopoietic–stromal dysregulation in myelofibrosis.

Taken together, our study establishes a humanized in vivo platform that faithfully models key aspects of human myelofibrosis and reveals a central role for SPP1/OPN-driven osteogenic and fibrotic remodeling downstream of aberrant THPO signaling. Targeting the SPP1 axis may therefore represent a promising therapeutic strategy aimed at restoring bone marrow niche function in myelofibrosis, complementing current treatments that primarily target malignant hematopoietic clones.

References

1. Nangalia, J. and A.R. Green, *Myeloproliferative neoplasms: from origins to outcomes.* Blood, 2017. **130**(23): p. 2475-2483.
2. Karagianni, A. and K. Ravid, *Myeloproliferative disorders and their effects on bone homeostasis: the role of megakaryocytes.* Blood, 2022. **139**(21): p. 3127-3137.
3. Reynolds, S.B., et al., *Exploring the Molecular Landscape of Myelofibrosis, with a Focus on Ras and Mitogen-Activated Protein (MAP) Kinase Signaling.* Cancers (Basel), 2023. **15**(18).
4. Passamonti, F. and B. Mora, *Myelofibrosis.* Blood, 2023. **141**(16): p. 1954-1970.
5. Benlabiod, C., et al., *Calreticulin del52 and ins5 knock-in mice recapitulate different myeloproliferative phenotypes observed in patients with MPN.* Nat Commun, 2020. **11**(1): p. 4886.
6. Li, J., et al., *Mouse models of myeloproliferative neoplasms: JAK of all grades.* Dis Model Mech, 2011. **4**(3): p. 311-7.
7. Pikman, Y., et al., *MPLW515L is a novel somatic activating mutation in myelofibrosis with myeloid metaplasia.* PLoS Med, 2006. **3**(7): p. e270.
8. Yan, X.Q., et al., *Chronic exposure to retroviral vector encoded MGDF (mpl-ligand) induces lineage-specific growth and differentiation of megakaryocytes in mice.* Blood, 1995. **86**(11): p. 4025-33.
9. Villeval, J.L., et al., *High thrombopoietin production by hematopoietic cells induces a fatal myeloproliferative syndrome in mice.* Blood, 1997. **90**(11): p. 4369-83.
10. Schneider, R.K., et al., *Gli1(+) Mesenchymal Stromal Cells Are a Key Driver of Bone Marrow Fibrosis and an Important Cellular Therapeutic Target.* Cell Stem Cell, 2017. **20**(6): p. 785-800 e8.
11. Li, H., et al., *Low/negative expression of PDGFR-alpha identifies the candidate primary mesenchymal stromal cells in adult human bone marrow.* Stem Cell Reports, 2014. **3**(6): p. 965-74.

12. Reinisch, A., et al., *Generation and use of a humanized bone-marrow-ossicle niche for hematopoietic xenotransplantation into mice.* Nat Protoc, 2017. **12**(10): p. 2169-2188.
13. Klement, J.D., et al., *Osteopontin Blockade Immunotherapy Increases Cytotoxic T Lymphocyte Lytic Activity and Suppresses Colon Tumor Progression.* Cancers (Basel), 2021. **13**(5).
14. Bianchi, E., et al., *Inhibition of ERK1/2 signaling prevents bone marrow fibrosis by reducing osteopontin plasma levels in a myelofibrosis mouse model.* Leukemia, 2023. **37**(5): p. 1068-1079.
15. Gaytan, F., et al., *A novel RGB-trichrome staining method for routine histological analysis of musculoskeletal tissues.* Sci Rep, 2020. **10**(1): p. 16659.
16. Mughal, Z., et al., *Megakaryocytic Clustering in Chronic Myeloid Leukemia: Can it be a Predictor of Clinical Outcome?* J Coll Physicians Surg Pak, 2021. **31**(1): p. 34-38.
17. Reinisch, A., et al., *A humanized bone marrow ossicle xenotransplantation model enables improved engraftment of healthy and leukemic human hematopoietic cells.* Nat Med, 2016. **22**(7): p. 812-21.
18. Yan, X.Q., et al., *A model of myelofibrosis and osteosclerosis in mice induced by overexpressing thrombopoietin (mpl ligand): reversal of disease by bone marrow transplantation.* Blood, 1996. **88**(2): p. 402-9.
19. Thiele, J., et al., *European consensus on grading bone marrow fibrosis and assessment of cellularity.* Haematologica, 2005. **90**(8): p. 1128-32.
20. Li, H., et al., *Identification of phenotypically, functionally, and anatomically distinct stromal niche populations in human bone marrow based on single-cell RNA sequencing.* Elife, 2023. **12**.
21. Nangalia, J. and A.R. Green, *Myeloproliferative neoplasms: from origins to outcomes.* Hematology Am Soc Hematol Educ Program, 2017. **2017**(1): p. 470-479.
22. Lacout, C., et al., *JAK2V617F expression in murine hematopoietic cells leads to MPD mimicking human PV with secondary myelofibrosis.* Blood, 2006. **108**(5): p. 1652-60.
23. Marty, C., et al., *Calreticulin mutants in mice induce an MPL-dependent thrombocytosis with frequent progression to myelofibrosis.* Blood, 2016. **127**(10): p. 1317-24.
24. Fosselteder, J., et al., *Human gene-engineered calreticulin mutant stem cells recapitulate MPN hallmarks and identify targetable vulnerabilities.* Leukemia, 2023. **37**(4): p. 843-853.
25. Flosdorf, N., et al., *Proinflammatory phenotype of iPS cell-derived JAK2 V617F megakaryocytes induces fibrosis in 3D in vitro bone marrow niche.* Stem Cell Reports, 2024. **19**(2): p. 224-238.
26. Kakumitsu, H., et al., *Transgenic mice overexpressing murine thrombopoietin develop myelofibrosis and osteosclerosis.* Leuk Res, 2005. **29**(7): p. 761-9.
27. Leimkuhler, N.B., et al., *Heterogeneous bone-marrow stromal progenitors drive myelofibrosis via a druggable alarmin axis.* Cell Stem Cell, 2021. **28**(4): p. 637-652 e8.
28. Banjanin, B., et al., *Wnt-dependent spatiotemporal reprogramming of bone marrow niches drives fibrosis.* Hemasphere, 2026. **10**(2): p. e70309.
29. Ruberti, S., et al., *Involvement of MAF/SPP1 axis in the development of bone marrow fibrosis in PMF patients.* Leukemia, 2018. **32**(2): p. 438-449.

Figure legend

Figure 1. Establishment of a humanized bone marrow microenvironment supporting human hematopoiesis. (A) Schematic representation of the experimental design for generating humanized ossicles and inducing myelofibrosis. (B) Hematoxylin and eosin (H&E) staining of a representative humanized ossicle. Left**:** overview of the ossicle structure; right**:** magnified view of the boxed region in the left panel. Scale bar, 100 µm. CB, cortical bone; TB, trabecular bone; HC, hematopoietic cells; a, adipocyte; v, vessel. (C) Immunohistochemical staining of the ossicle using an antibody against human mitochondria (brown). Red arrows indicate human mitochondria–positive cells. (D) Representative flow cytometry plots showing human $CD45^+$ cells among viable cells isolated from ossicles eight weeks after intraossicle transplantation of 3×10^5 human bone marrow $CD34^+$ cells. (E) Quantification of the percentage of human $CD45^+$ cells in ossicles ($n = 8$) compared with murine femurs ($n = 5$). **: $p < 0.01$ (Mann-Whitney test).

Figure 2. THPO overexpression induces a skewed myeloid/lymphoid ratio and megakaryocyte dysplasia in humanized ossicles. (A) Representative FACS plots (left and middle panels) showing human $CD45^+$ cells in GFP and THPO ossicles 8 weeks after intraossicle transplantation. Right panel: Quantification of the fold change in the frequency of human $CD45^+$ cells in THPO ossicles relative to GFP controls 8 weeks post-transplantation (median indicated, GFP: n=15, THPO: n=15). (B) Representative FACS plots (left and middle panels) showing human $CD15^+CD33^+CD66b^+$ cells versus $CD19^+$ cells in GFP and THPO ossicles 8 weeks after intraossicle transplantation. Right panel: Quantification of the myeloid to lymphoid ratio in THPO ossicles relative to GFP controls 8 weeks post-transplantation (median indicated, GFP: n=13, THPO: n=13). (C) Representative FACS plots (left and middle panels) showing human $CD41a^+$ cells versus $CD42b^+$ cells in GFP and THPO ossicles 8 weeks after intraossicle transplantation. Right panel: Quantification of the

fold change in the frequency of human $CD41a^+CD42b^+$ cells in THPO ossicles relative to GFP controls 8 weeks post-transplantation (median indicated, GFP: *n* =9, THPO: n=9). (D) Dual-color immunohistochemical (IHC) staining of ossicles showing human mitochondria (brown) and human CD45 (red). Red arrows indicate human megakaryocytes in GFP and THPO ossicles. Scale bar: 50 µm. (E) Quantification of megakaryocytes per ossicle. **(F)** H&E staining of GFP and THPO ossicles. Left panel: Megakaryocyte clusters are indicated by black circles. Scale bar: 50 µm. Right panel: Quantification of megakaryocyte clusters per ossicle. (**p = 0.0014, Mann-Whitney test).

Figure 3. THPO overexpression induces fibrosis in huMF ossicles. (A) Representative images of Gordon and Sweet's reticulin staining of GFP and THPO ossicles 8 weeks post-transplantation. Scale bar indicates 20 µm. (B) Blinded fibrosis grading was performed independently by two observers. Dot plot showing the fibrosis grade of individual ossicles (n = 15 for GFP and n = 14 for THPO). Statistical comparisons were performed using the Mann–Whitney test. *p< 0.05

Figure 4. THPO overexpression induces migration of human hematopoietic cells from ossicles. (A) Representative FACS plots (left and middle panels) showing human $CD45^+$ cells in femurs from GFP and THPO groups 8 weeks after intraossicle transplantation. The right panel summarizes the fold change in the frequency of human $CD45^+$ cells in femurs of the THPO group relative to GFP controls at 8 weeks post-transplantation (median indicated; n = 6 per group). (B) Representative FACS plots (left and middle panels) showing human $CD45^+$ cells in spleens from GFP and THPO groups 8 weeks after intraossicle transplantation. The right panel summarizes the fold change in the frequency of human $CD45^+$ cells in spleens of the THPO group relative to GFP controls at 8 weeks post-transplantation (median indicated; n = 9 per group). *p < 0.05 (Mann-Whitney test). (C) Spleen-to-body weight ratio (median indicated; GFP: n = 9, THPO: n = 8).

Figure 5. THPO overexpression induces microenvironmental remodeling in humanized ossicles. (A) Representative H&E-stained images of GFP and THPO ossicles at 8 weeks post-transplantation. Scale bar: 1 mm. (B) Quantification of the fold change in the bone area relative to the total ossicle area in THPO ossicles compared with GFP controls (median indicated; GFP: n = 10, THPO: n = 9; **p = 0.0001, Mann-Whitney test). (C) Quantification of the fold change in trabecular bone relative to the ossicle cavity area (median indicated; GFP: n = 8, THPO: n = 9; *p = 0.0244, Mann-Whitney test). (D) Representative RGB staining of GFP and THPO ossicles. Scale bar: 500 µm. (E) Quantification of the fold change in osteoid area within the ossicle (median indicated; GFP: n = 6, THPO: n = 6).

Figure 6. Anti-SPP1 neutralizing antibody treatment reduces fibrosis and attenuates the skewed myeloid-to-lymphoid ratio in huMF ossicles. (A) Representative images of CD56 and SPP1 immunostaining in GFP and THPO ossicles. (B) Quantification of CD56 and SPP1 expression in GFP and THPO ossicles. (C) Representative images of CD56 and SPP1 immunostaining in bone marrow biopsies from healthy donors and patients with primary myelofibrosis (PMF). (D) Quantification of CD56 and SPP1 expression in healthy donor and PMF bone marrow biopsies. (E) Quantification of the fold change in the myeloid-to-lymphoid ratio in THPO ossicles following treatment with anti-SPP1 antibody or IgG control, relative to GFP controls. (F) Quantification of the fold change in the percentage of $CD41^+$ cells in THPO ossicles following treatment with anti-SPP1 antibody or IgG control, relative to GFP controls. *$p < 0.05$ (Kruskal-Wallis test). (G) Quantification of fibrosis grades in THPO ossicles after treatment with anti-SPP1 antibody or IgG control, compared with GFP controls. P values are indicated on top of comparison bars. (H) Quantification of the percentage of human $CD45^+$ cells in the spleens of THPO ossicle–bearing mice following treatment with anti-SPP1 antibody or IgG control, compared with GFP ossicle–bearing mice.

(I) Quantification of the fold change in the bone-to-ossicle area ratio in THPO ossicles following treatment with anti-SPP1 antibody or IgG control, relative to GFP controls.

Figure 1

A

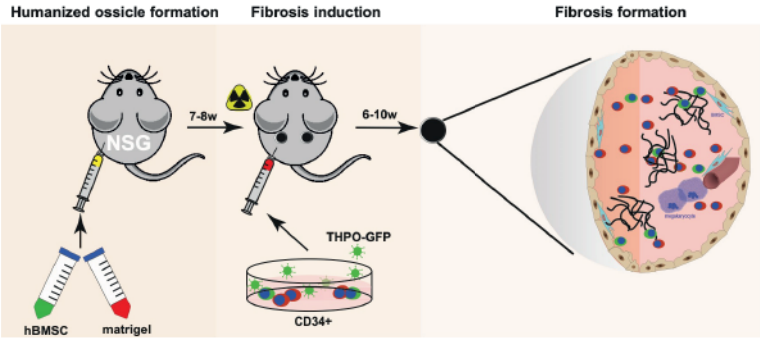

B

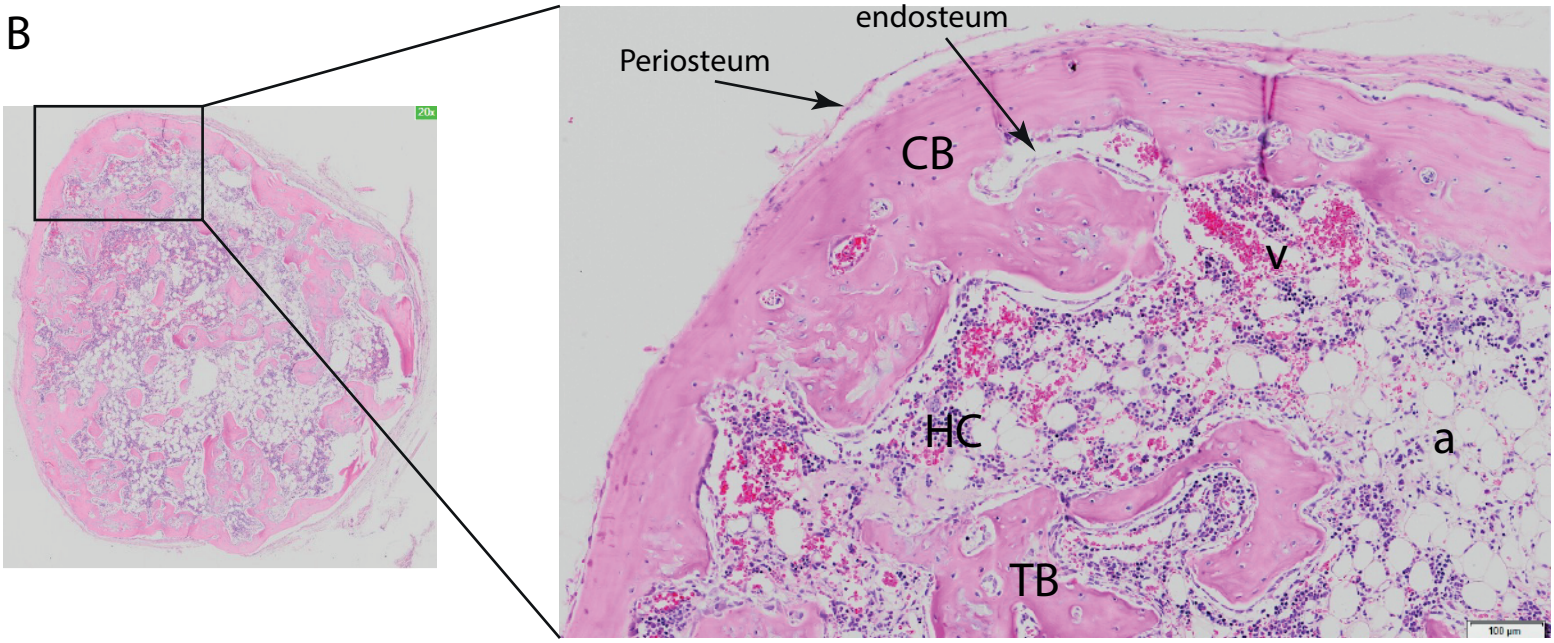

C

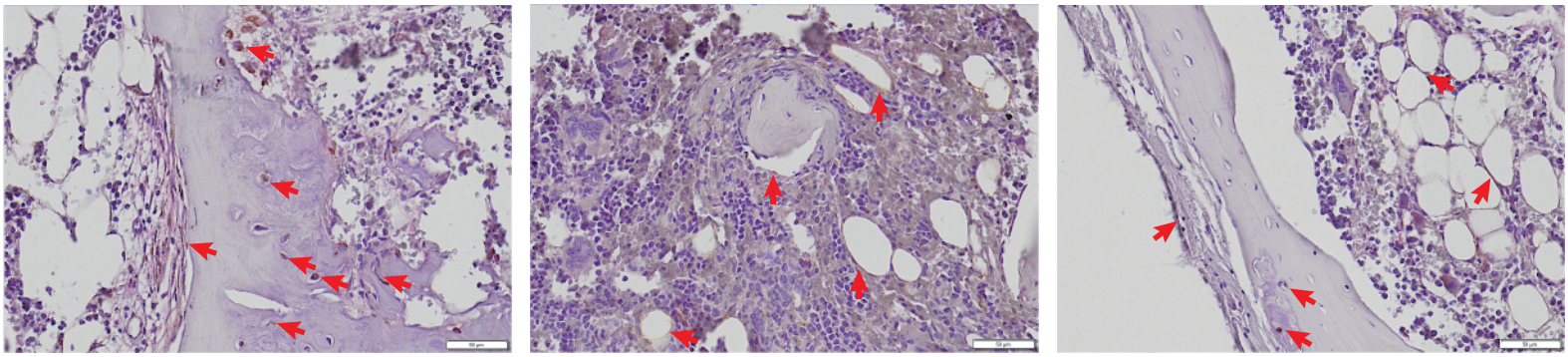

D

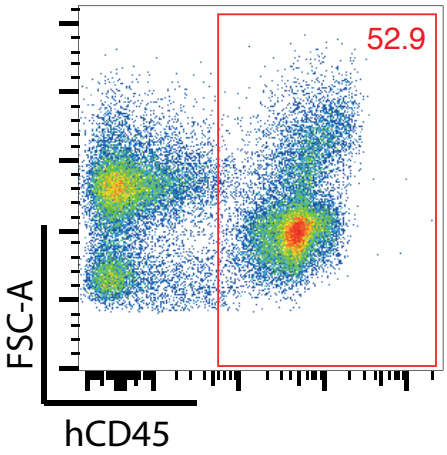

E

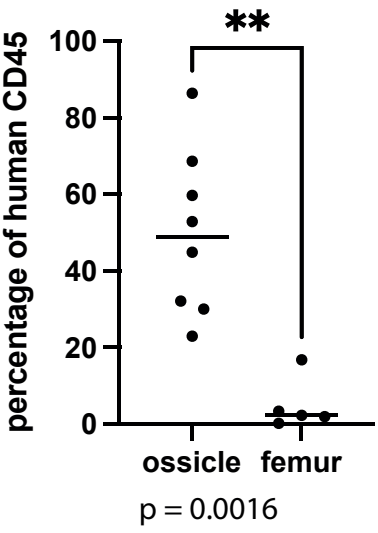

Figure 2

A

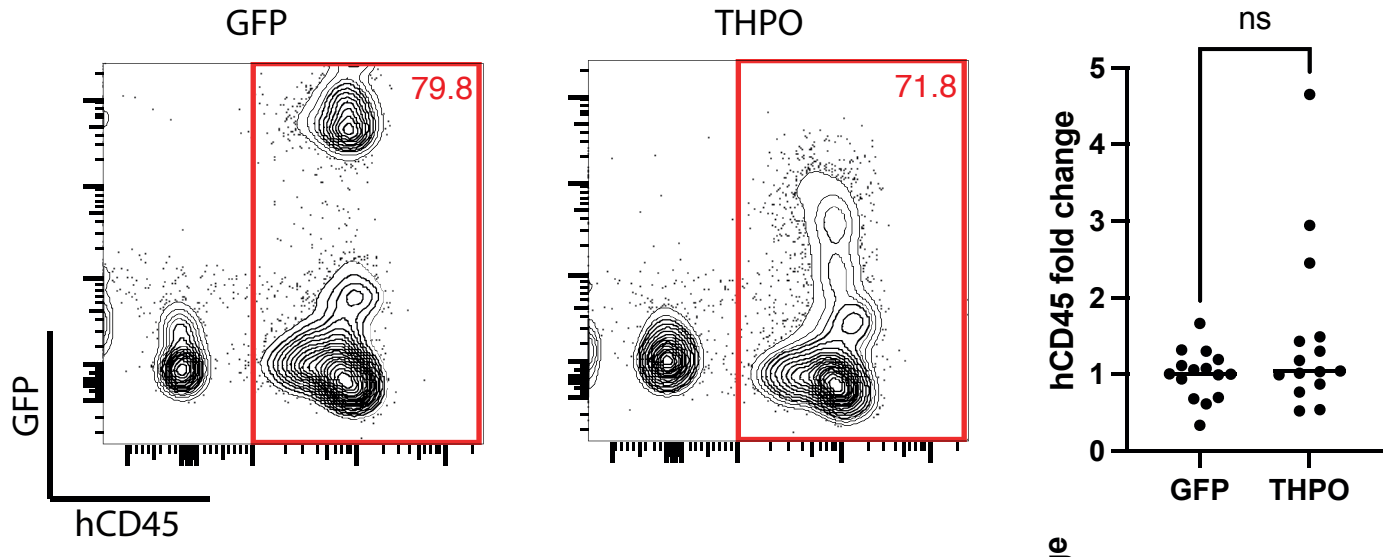

B

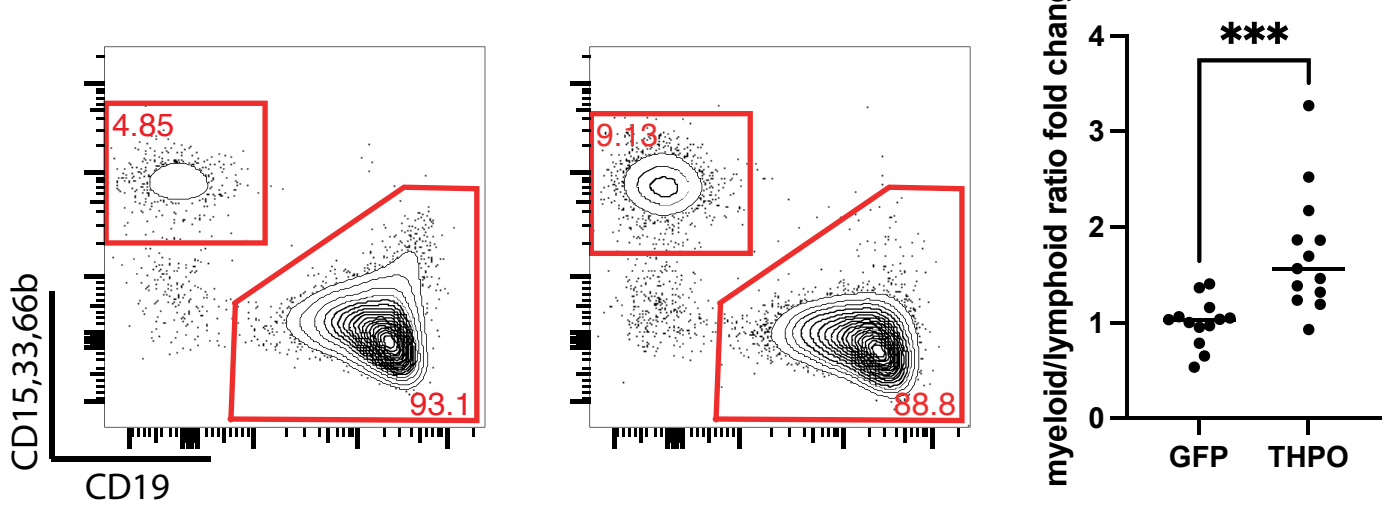

C

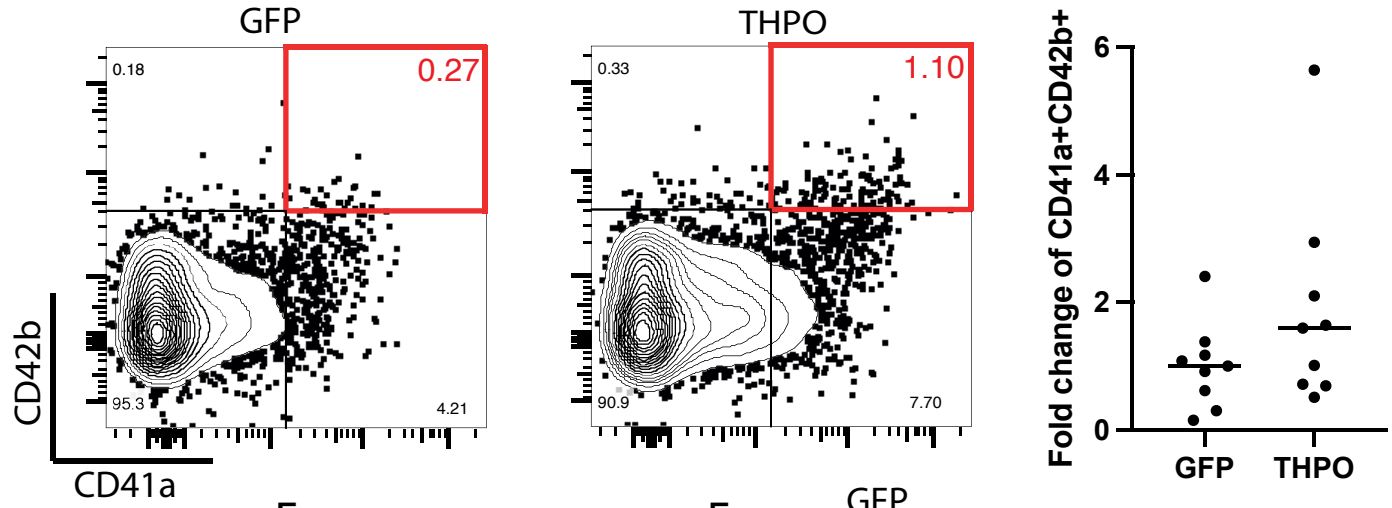

D

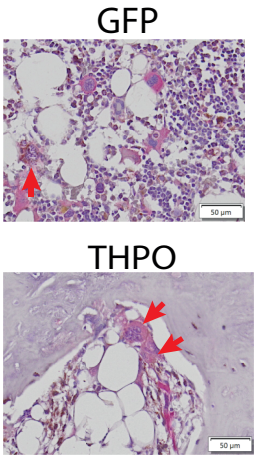

E

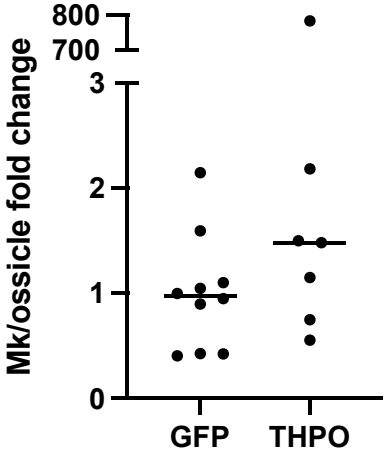

F

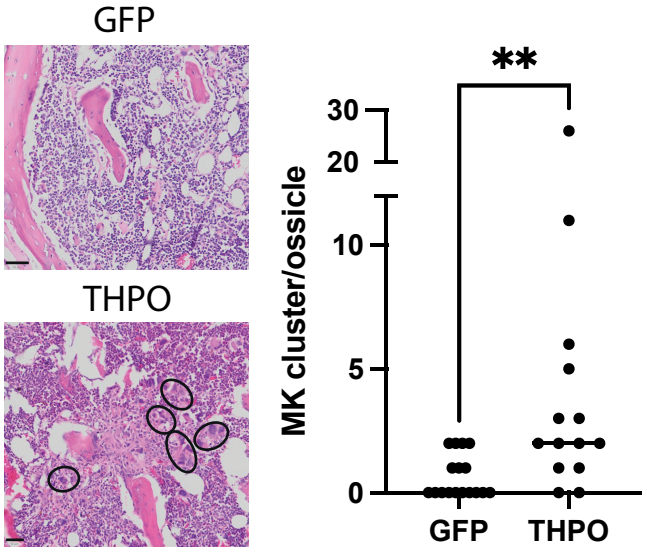

Figure 3

A

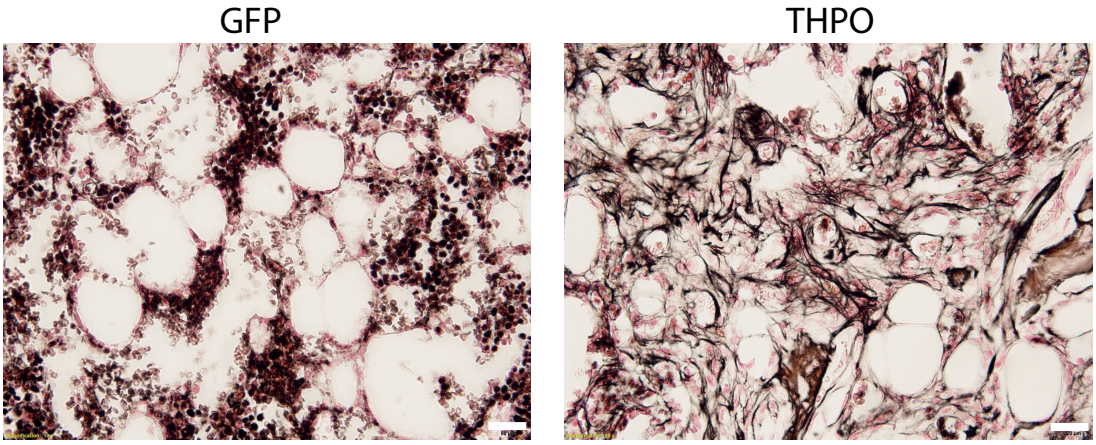

B

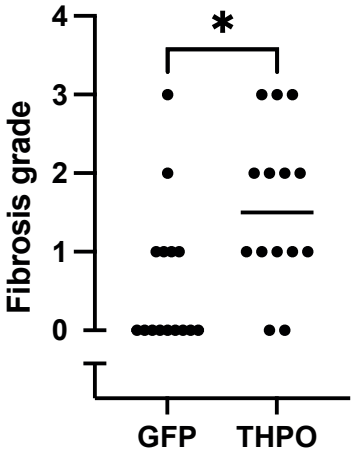

Figure 4

A

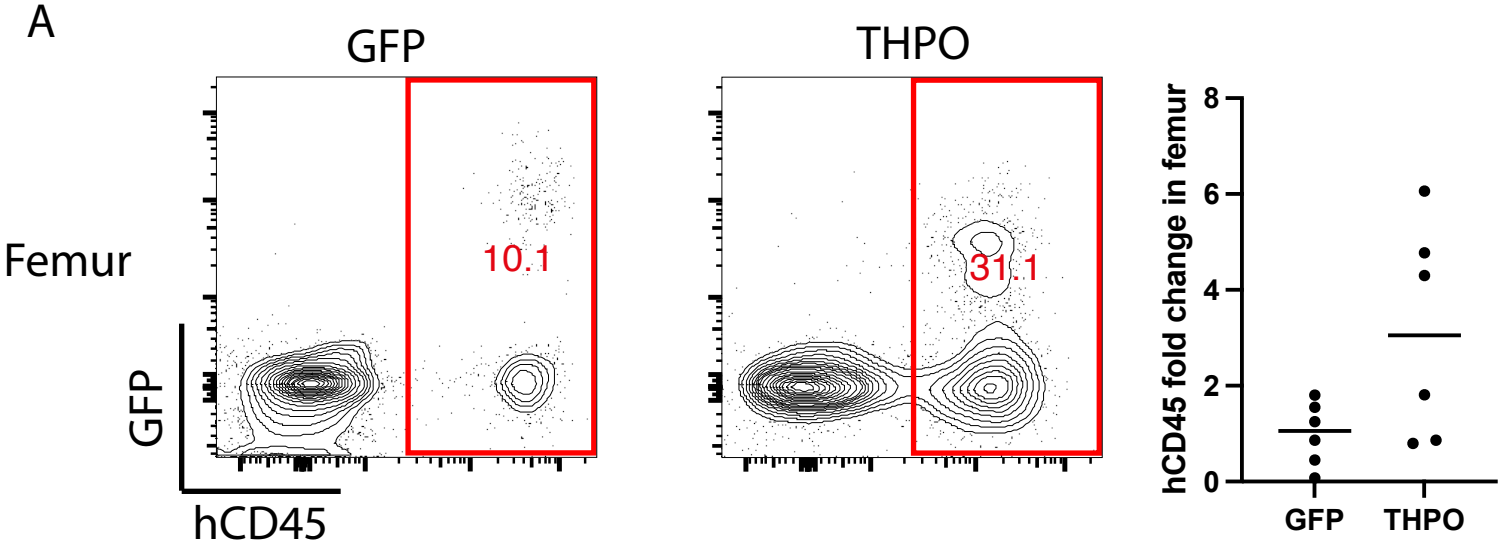
GFP
THPO
Femur
10.1
31.1
GFP
hCD45
hCD45 fold change in femur
8
6
4
2
0
GFP
THPO

B

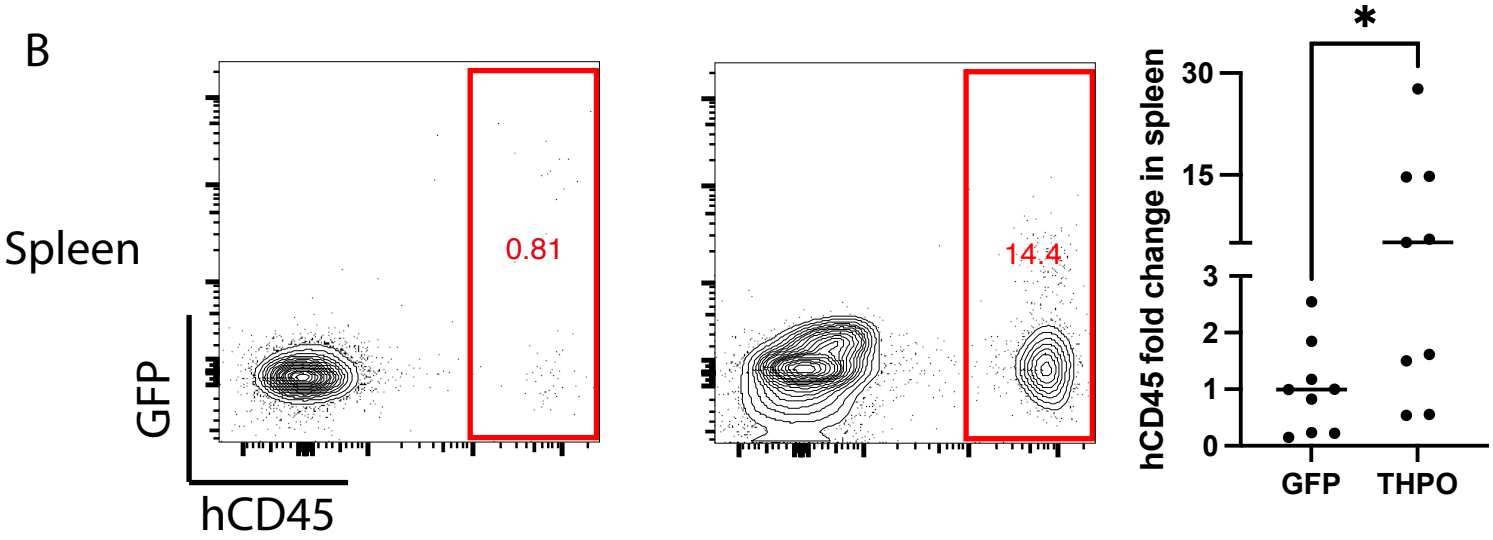
Spleen
0.81
14.4
GFP
hCD45
hCD45 fold change in spleen
*
30
15
3
2
1
0
GFP
THPO

C

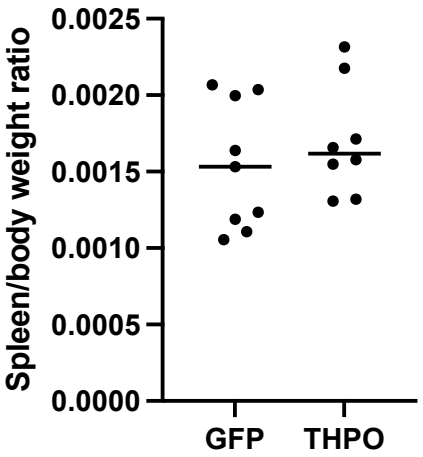
Spleen/body weight ratio
0.0025
0.0020
0.0015
0.0010
0.0005
0.0000
GFP
THPO

Figure 5

A

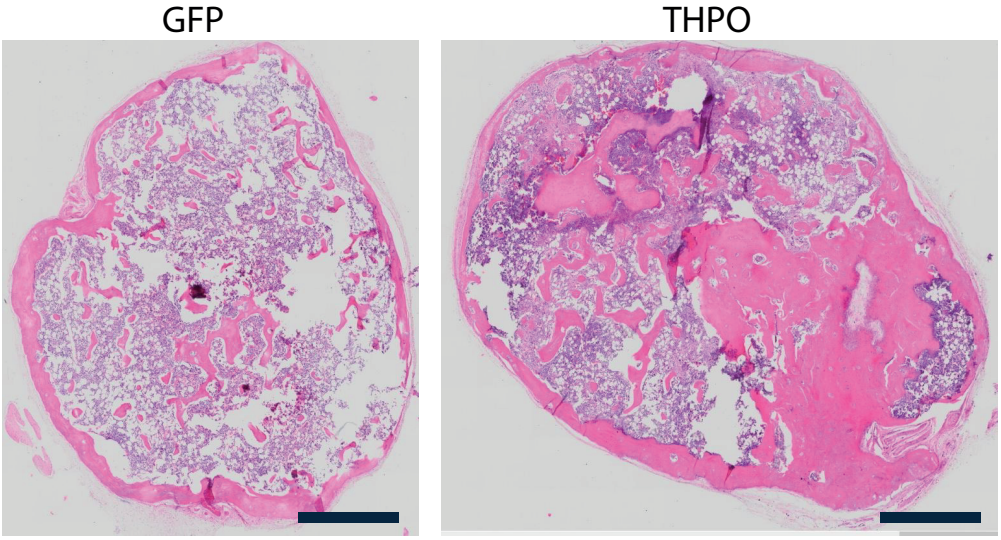

B

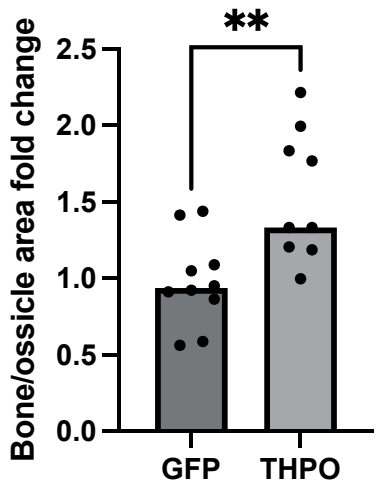

C

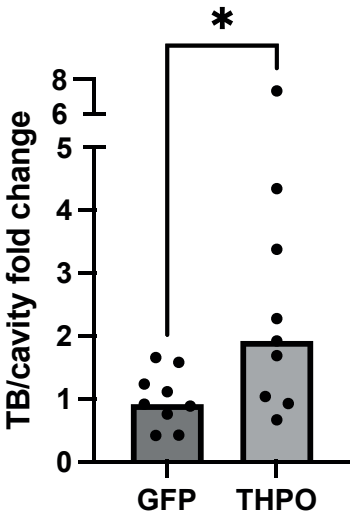

D

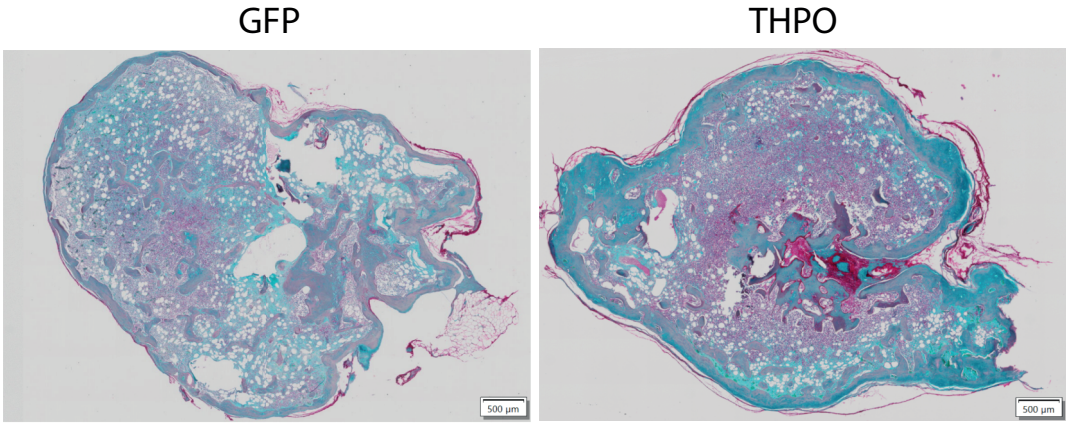

E

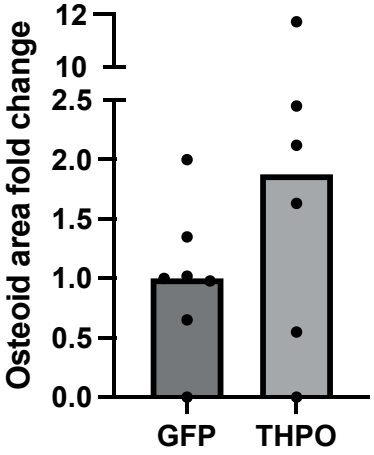

Figure 6

A

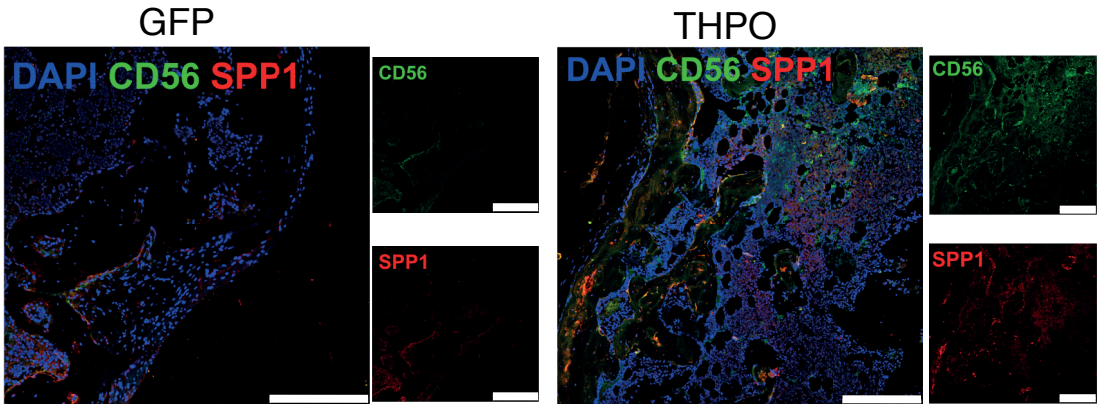

B

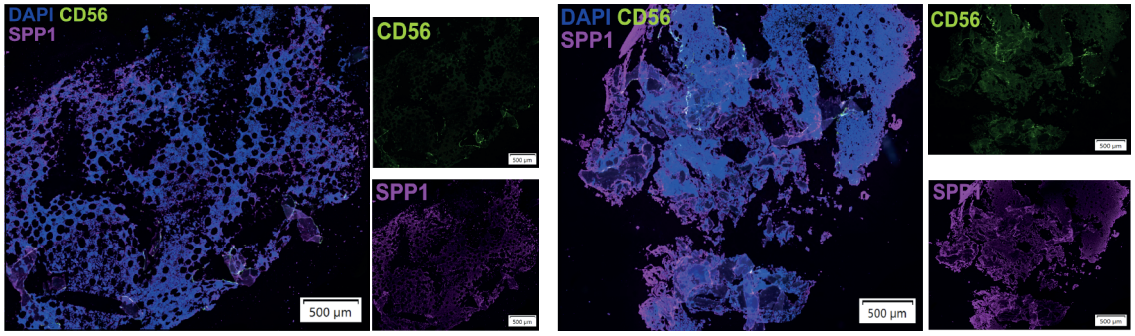

C

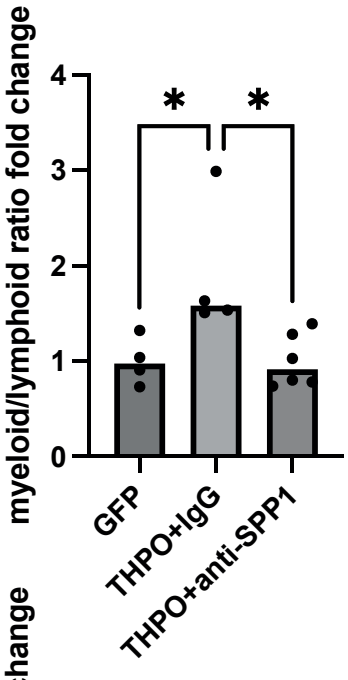

D

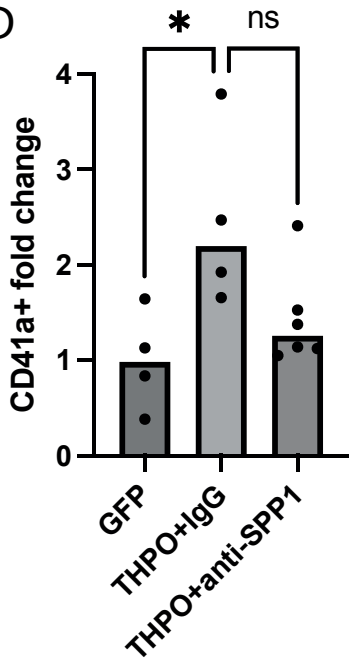

E

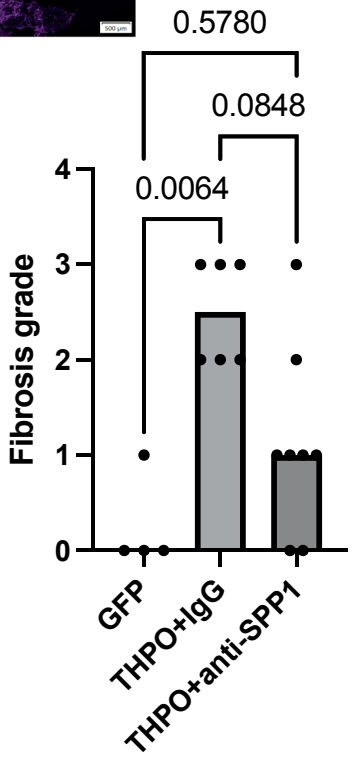

F

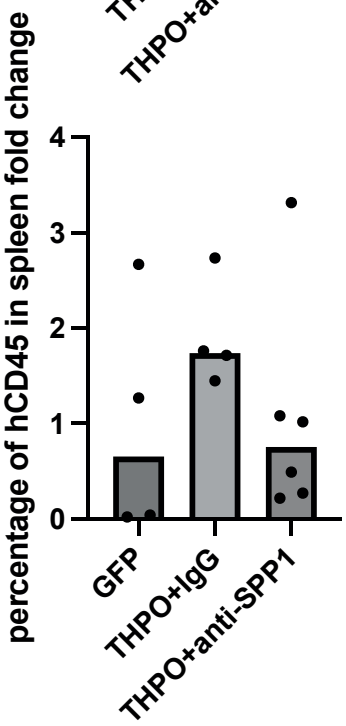
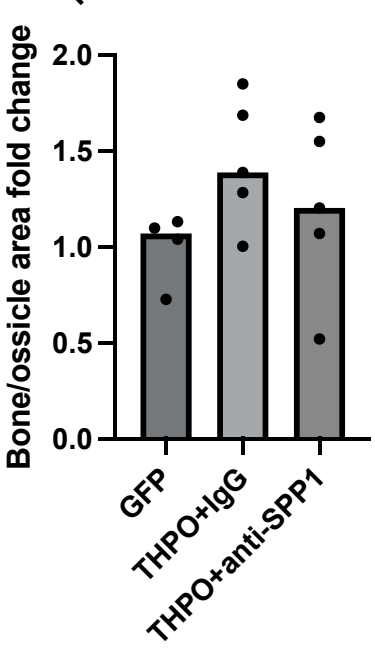
G